

# Rational Design of Mixed Polyanion Electrodes $\text{Na}_x\text{V}_2\text{P}_{3-i}(\text{Si/S})_i\text{O}_{12}$ for Sodium Batteries

Published as part of the Virtual Special Issue “John Goodenough at 100”.

Vishakha Kapoor,<sup>#</sup> Baltej Singh,<sup>#</sup> Gopalakrishnan Sai Gautam, Anthony K. Cheetham, and Pieremanuele Canepa\*



Cite This: <https://doi.org/10.1021/acs.chemmater.2c00230>



Read Online

ACCESS |



Metrics & More

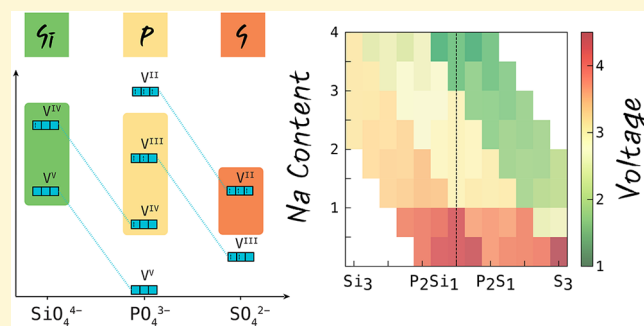


Article Recommendations



Supporting Information

**ABSTRACT:** Polyanion-based electrode materials are important for rechargeable sodium(Na)-ion batteries owing to their structural stability and their high redox voltage. The redox voltages and gravimetric capacities of polyanion electrodes can be tuned by the choice of transition metal and/or polyanion groups. In this work we explore the effect of changing polyanion groups on the redox voltages and the gravimetric capacities of polyanion electrodes. Using first-principles calculations, we examine the influence of polyanionic substitutions on the stability and electrochemical behavior of the  $\text{Na}_3\text{V}_2(\text{PO}_4)_3$  electrode material, which adopts the prototype structure of the sodium superionic conductor (NaSICON). Starting from the  $\text{Na}_3\text{V}_2(\text{PO}_4)_3$  structure, we explore the partial or total substitution of  $\text{PO}_4^{3-}$  groups by  $\text{SiO}_4^{4-}$  or  $\text{SO}_4^{2-}$  moieties, unveiling the uncharted multicomponent Na–V–P–(Si/S)–O phase diagram. We show that small amounts of  $\text{SiO}_4^{4-}$  can activate the  $\text{V}^{\text{V/IV}}$  redox couple, which is not experimentally accessible in the  $\text{PO}_4^{3-}$  NaSICON analogue, thereby increasing the average Na intercalation voltage. In the case of  $\text{SO}_4^{2-}$  substitution, we observe an increase in voltage of each V redox couple (i.e.,  $\text{V}^{\text{III/II}}$ ,  $\text{V}^{\text{IV/III}}$ , and  $\text{V}^{\text{V/IV}}$ ) but at the expense of the maximum amount of  $\text{Na}^+$  intercalated. We show that exploiting the varying inductive effects of different polyanion groups can be effective for tuning the energy density of NaSICON electrode materials.



## 1. INTRODUCTION

With their exceptional energy densities, lithium (Li)-ion batteries dominate the growing market of portable energy storage devices and electric vehicles. Yet, due to the geopolitically constrained supply chains of Li and crucial transition metals (e.g., cobalt and nickel), further expansion in the use of Li-ion cells is at risk.<sup>1–3</sup> To accommodate the ever increasing global energy consumption and a transition to clean energy, large-scale and cost-effective energy storage technologies that provide an alternative to Li-ion are needed.

With a “rocking chair” architecture analogous to that of Li-ion cells, the sodium (Na)-ion battery is a promising, beyond-Li-ion storage technology, with several advantages. The ubiquity of Na makes it approximately 50 times cheaper than Li.<sup>1,4</sup> Also, Na-ion batteries utilize inexpensive aluminum current collectors. Na-ion cells can be fabricated using processes similar to those of Li-ion batteries, which may ease the transition toward the use of sodium.<sup>4,5</sup> Thus, the development of Na-ion batteries has grown rapidly,<sup>4,6</sup> accompanied by a surge of interest in safer solid-state batteries relying on Na ions.<sup>7–10</sup> Nevertheless, Na has a lower (in magnitude) electrochemical potential of  $-2.71$  V vs the

standard hydrogen electrode (SHE) and a higher atomic mass of 22.99 a.m.u. compared to that of Li ( $-3.04$  V vs SHE and 6.94 a.m.u., respectively), typically resulting in lower energy densities in Na-ion vs Li-ion cells.<sup>11</sup>

To improve the electrochemical performance of Na-ion batteries, it is necessary to develop electrode materials with enhanced operating voltages and capacities and minimal structural changes during electrochemical cycling.<sup>11</sup> Due to a higher proportion of Na per formula unit, layered transition metal oxides may show the largest gravimetric capacities, but their practical use as an electrode is limited by irreversible structural phase transitions during electrochemical cycling.<sup>12</sup> In contrast, polyanionic frameworks incorporating  $\text{SO}_4^{2-}$ ,  $\text{PO}_4^{3-}$ , and  $\text{SiO}_4^{4-}$  groups<sup>13–16</sup> can reversibly intercalate Na ions at relatively high operating voltages (which is attributed to the

Received: January 24, 2022

Revised: March 17, 2022

inductive effect of the polyanionic moieties, see below)<sup>14,17,18</sup> but yield lower capacities due to the additional mass of the polyanionic groups. Therefore, polyanion electrodes result in energy densities that are similar to or lower than those of layered oxide materials.<sup>13,14,19,20</sup> However, polyanion compounds also display robust 3D frameworks, limiting their expansion/contraction during Na intercalation, thus increasing the safety and reversibility of the electrochemical setup<sup>21,22</sup> and making them an important family of Na cathodes.

The sodium superionic conductor (NaSICON) is a class of polyanion materials of general formula  $\text{Na}_x\text{M}_2(\text{ZO}_4)_3$ ,<sup>23,8,14,24–29</sup> where M is a single (or multiple) redox-active transition metal(s) and  $\text{ZO}_4$  is a polyanionic group (Z is usually  $\text{Si}^{4+}$ ,  $\text{P}^{5+}$ , and/or  $\text{S}^{6+}$ , but other cations, such as  $\text{Mo}^{6+}$  and  $\text{W}^{6+}$ , are possible).<sup>18,17,14,22,30,28</sup> In  $\text{Na}_x\text{M}_2(\text{ZO}_4)_3$ , the Na concentration,  $x$ , can vary from 1 to 4, depending on the oxidation states of the cations M and Z.

Here, we explore strategies for tuning the  $\text{ZO}_4$  groups to obtain high-energy-density NaSICON electrodes by enhancing the Na-intercalation voltage and/or the gravimetric capacity. We have considered the NaSICON framework of  $\text{Na}_3\text{V}_2(\text{PO}_4)_3$  and explored the substitution of  $\text{PO}_4^{3-}$  groups with  $\text{SiO}_4^{4-}$  or  $\text{SO}_4^{2-}$ . We chose  $\text{Na}_3\text{V}_2(\text{PO}_4)_3$  due to the presence of multiple oxidation states of V (2+, 3+, 4+, and 5+), the highly reversible Na-ion (de)intercalation, namely, the reversible extraction of 2  $\text{Na}^+$  at  $\sim 3.4$  V ( $\text{V}^{\text{IV/III}}$ ) to form  $\text{Na}_1\text{V}_2(\text{PO}_4)_3$ , and reversible insertion of 1  $\text{Na}^+$  at  $\sim 1.6$  V ( $\text{V}^{\text{III/II}}$ ) forming  $\text{Na}_4\text{V}_2(\text{PO}_4)_3$ .<sup>31–33,26,34–36,29</sup> We use the nomenclature  $\text{Na}_x\text{VP}_3$  for  $\text{Na}_x\text{V}_2(\text{PO}_4)_3$ ; for example,  $\text{Na}_3\text{VP}_3$  indicates  $\text{Na}_3\text{V}_2(\text{PO}_4)_3$  or  $\text{Na}_3\text{V}_2\text{P}_3\text{O}_{12}$ . Similarly,  $\text{Na}_x\text{VP}_{1.5}\text{S}_{1.5}$  indicates a composition of  $\text{Na}_x\text{V}_2\text{P}_{1.5}\text{S}_{1.5}\text{O}_{12}$ . We will refer to the  $\text{Na}_x\text{VP}_3$  formula/structural unit as NaSICON.

The average voltages of NaSICON frameworks follow the standard reduction potentials of the transition metals present,<sup>14,24</sup> with the intercalation voltage increasing as the higher (possible) oxidation states of the transition metals accessed (e.g.,  $\text{V}^{\text{IV/III}}$  exhibits a higher voltage than  $\text{V}^{\text{III/II}}$ ). Alternatively, the voltage of an existing transition metal redox couple (e.g.,  $\text{V}^{\text{IV/III}}$ ) can be increased by reducing the degree of covalency of the V–O bond via modification of the polyanion units, i.e., by changing the Z–O bonding in  $\text{ZO}_4$ . This voltage increase is caused by the inductive effect exerted by the Z cation on the Z–O bond, as defined in the framework of molecular orbital theory.<sup>18,37</sup> Specifically, Z cations with higher oxidation states draw O electrons away from the M atom, thus lowering the covalency (or increasing the ionicity) of the M–O bonds and raising the redox voltages upon Na (de)-intercalation. Therefore, one can modulate the intercalation voltage by changing the Z cation. Only a handful of studies have been performed on varying the Z species, for example, by substituting  $\text{PO}_4^{3-}$  groups by  $\text{SiO}_4^{4-}$  in  $\text{Na}_x\text{VP}_3$ .<sup>8,38–40,16,41</sup> However, the effects of substitution of diverse polyanion units on the phase stability of  $\text{Na}_3\text{VP}_3$ , the electrochemical behavior, and the Na ion kinetics are far from being fully addressed.

Our study systematically explores the phase stability of  $\text{Na}_x\text{VP}_3$  upon partial (or full) exchange of the  $\text{P}^{5+}$  sites with other cation species, specifically  $\text{Si}^{4+}$  or  $\text{S}^{6+}$ . Our choice of replacing P with Si is largely motivated by the work of Hong and Goodenough, where the authors mixed Si and P to enhance the Na-ion conductivity in Zr-based NaSICON solid electrolytes.<sup>8,23</sup> We consider S substitution since previous studies have shown that the  $\text{SO}_4^{2-}$  group enhances the redox voltage of the  $\text{Fe}^{\text{III/II}}$  redox couple from 2.8 V (for  $\text{SiO}_4^{4-}$ ) to

3.6 V vs  $\text{Li}^+/\text{Li}^-$  (for  $\text{SO}_4^{2-}$ ) in Li-based NaSICON cathodes.<sup>17,37</sup>

We use density functional theory (DFT) calculations coupled with a robust thermodynamic framework to reveal the effects of Si or S substitutions on the  $\text{Na}_x\text{VP}_3$  structure, namely, its thermodynamic stability and Na intercalation voltages.<sup>42,43</sup> The computed multicomponent phase diagrams of Na–V–P–Si/S–O are used to examine the synthesizability of Si/S substituted  $\text{Na}_x\text{VP}_3$  at varying Na contents. Before analyzing the effects of Si/S substitution, we provide an overview of the structure and Na intercalation properties in  $\text{Na}_x\text{VP}_3$ . Our analysis provides important guiding principles for future experimental synthesis of mixed polyanion NaSICON materials for high-energy-density Na-ion batteries.

## 2. STRUCTURE AND Na INTERCALATION IN $\text{Na}_x\text{V}_2(\text{PO}_4)_3$

To benchmark our methodology and provide context for the study of mixed polyanion vanadium NaSICONs, we briefly revisit the mechanism of Na intercalation in  $\text{Na}_x\text{VP}_3$ . The rhombohedral ( $R\bar{3}c$ ) and monoclinic ( $C2/c$ ) NaSICON phases of  $\text{Na}_x\text{VP}_3$  can be understood as networks of “lantern” units stacked into columns perpendicular to the basal plane to form the NaSICON framework (Figure S2).<sup>23,31,44,45</sup> Each lantern unit (see inset of Figure 1) consists of two  $\text{VO}_6$  octahedra

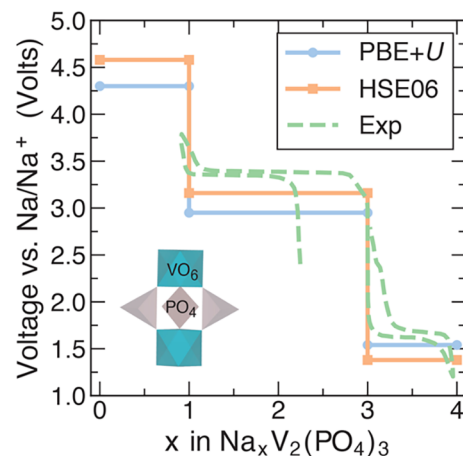


**Figure 1.** Comparison of the experimental (Exp) and predicted voltage curves of  $\text{Na}_x\text{VP}_3$ .<sup>24,31</sup> Theoretical predictions with the PBE +  $U$  (blue lines and symbols) and the HSE06 hybrid (orange lines and symbols) functionals. The inset displays the lantern units of the NaSICON framework for  $\text{Na}_x\text{VP}_3$ , which are made up of  $\text{VO}_6$  octahedra (cyan) and  $\text{PO}_4$  tetrahedra (gray).

corner-sharing with O atoms of three  $\text{PO}_4$  tetrahedra. Each O atom in the structure is shared between  $\text{VO}_6$  and  $\text{PO}_4$  in this manner, forming a three-dimensional (3-D) framework with V–O–P bonding.

In the rhombohedral NaSICON, Na ions intercalate in two different sites: Na1 (6 coordinated) between the lantern units running along the  $c$ -axis and Na2 (8 coordinated) occupying interstitial spaces between parallel columns of lantern units. There are 1 Na1 and 3 Na2 sites per formula unit of  $\text{Na}_x\text{VP}_3$ . At room temperature, the rhombohedral  $\text{Na}_3\text{VP}_3$  phase distorts into the monoclinic structure, which gives rise to site splitting among the Na2 sites.<sup>25,46</sup>

The average Na intercalation voltage curves, as calculated with the Hubbard  $U$  corrected Perdew–Burke–Ernzerhof

(PBE+*U*)<sup>47,48</sup> functional and the Heyd–Scuseria–Ernzerhof (HSE06) hybrid functional<sup>49</sup> (see [Theoretical Methods](#) section), are compared in [Figure 1](#) with experimental curves at room temperature across the composition range  $1 \leq x \leq 4$  in  $\text{Na}_x\text{VP}_3$ .<sup>31</sup> The predicted voltages underestimate the experimental voltages, with the degree of underestimation being lower for PBE+*U* in the  $3 \leq x \leq 4$  range. In general, from [Figure 1](#) the average voltage and voltage difference are better predicted by the HSE06 hybrid functional. However, both functionals do obtain the correct qualitative trends in voltages, namely, the voltage plateaus between  $x = 1$  and  $x = 3$  and between  $x = 3$  and  $x = 4$ , both of which are indicative of two-phase behavior.<sup>50,51</sup> So, given the higher computational costs of the hybrid DFT HSE06, we have used the PBE+*U* functional for the remaining DFT calculations presented in this work.

According to previous experimental and computational investigations in  $\text{Na}_x\text{VP}_3$ , the stable phases are at  $x = 1, 3$ , and  $4$ , which are the ground state structures in the convex hull of [Figure S1](#) in the Supporting Information (SI). The voltage plateau between  $x = 1$  and  $x = 3$  is associated with the  $\text{V}^{\text{IV/III}}$  redox couple, while the  $\text{V}^{\text{III/II}}$  redox is active between  $x = 3$  and  $x = 4$ . Our PBE+*U* voltage plateaus, which are at  $\sim 2.9$  V and  $\sim 1.5$  V vs  $\text{Na}/\text{Na}^+$ , verify the  $\text{V}^{\text{IV/III}}$  and  $\text{V}^{\text{III/II}}$  redox couples (while being lower than the experimental values of  $\sim 3.4$  V and  $\sim 1.6$  V).<sup>31</sup> We use the computed magnetic moments to verify the existence of different oxidation states of V in our calculations. For example, at  $x = 1$ , we observe all V atoms in the  $\text{Na}_1\text{VP}_3$  structure to exhibit a magnetic moment of  $1.03 \mu_B$  reflecting  $\text{V}^{\text{IV}}$ , while at  $x = 3$ , the uniform magnetic moment of  $1.89 \mu_B$  corresponds to  $\text{V}^{\text{III}}$ . At  $x = 4$ ,  $\text{Na}_4\text{VP}_3$  turns metallic and electronic delocalization occurs over all of the vanadium redox centers, preventing us from distinguishing  $\text{V}^{\text{III}}$  and  $\text{V}^{\text{II}}$ .<sup>26</sup>

Recent studies using SCAN+*U* functionals<sup>26,29</sup> have isolated, both computationally and experimentally, an intermediate  $\text{Na}_2\text{VP}_3$  phase, which challenges the notion of a two-phase reaction between  $\text{Na}_3\text{VP}_3$  and  $\text{Na}_1\text{VP}_3$ , as predicted by PBE+*U*. However, our DFT calculations are consistent with those of Wang et al.<sup>26</sup> in suggesting that the extraction of Na between  $x = 4$  and  $1$  occurs exclusively from the Na2 sites, with the Na1 sites being electrochemically inactive. Further, the extraction of the last Na from  $\text{Na}_1\text{VP}_3$  occurs through the  $\text{V}^{\text{V/IV}}$  redox pair and corresponds to the extraction of sodium from the Na1 site in the structure. The extraction of the final Na has been claimed experimentally by chemical oxidation, but the experiment has never been reproduced.<sup>52</sup> The extraction of the last sodium (at the Na1 site) from  $\text{Na}_1\text{VP}_3$  has never been observed electrochemically due to the unfeasibly high voltage of  $>4.7$  V vs  $\text{Na}/\text{Na}^+$ <sup>53</sup> (the computationally predicted voltage is  $\sim 4.3$  V, [Figure 1](#)).

### 3. RATIONAL DESIGN OF HIGH-ENERGY DENSITY NaSICON ELECTRODES

Using  $\text{Na}_3\text{VP}_3$  as a starting compound, we have explored the composition space with respect to partial and full aliovalent substitution of  $\text{P}^{5+}$  with  $\text{Si}^{4+}$  or  $\text{S}^{6+}$ , respectively, as illustrated in [Figure 2](#). When tetrahedrally coordinated by O,  $\text{Si}^{4+}$  and  $\text{S}^{6+}$  exhibit markedly different ionic radii ( $r[\text{Si}^{4+}] \sim 26$  pm,  $r[\text{S}^{6+}] \sim 12$  pm) compared to that of P ( $r[\text{P}^{5+}] \sim 17$  pm).<sup>54</sup> Previous studies suggest that Si or S can replace P partially without introducing a significant degree of structural distortion in the NaSICON framework.<sup>8,23</sup> Nevertheless, the maximum amount

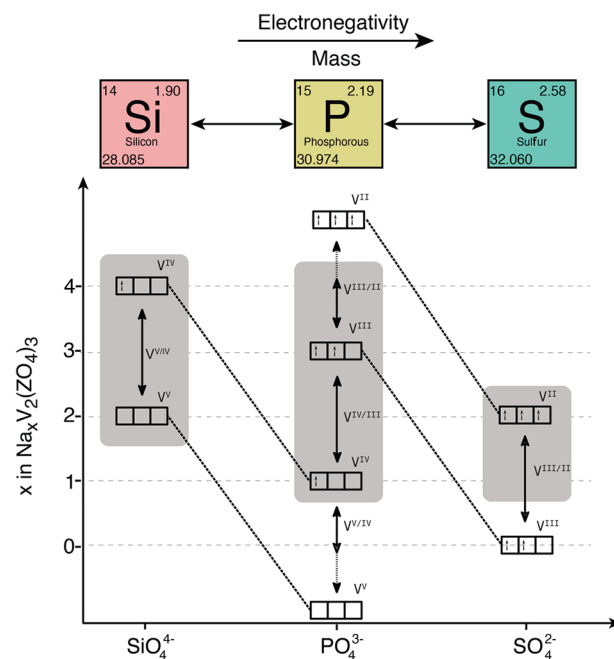


**Figure 2.** Physically accessible oxidation states and the electronic configurations of the  $t_{2g}$  orbitals of the vanadium centers as a function of Na concentration ( $x$ ) in  $\text{Na}_x\text{VP}_3$  with respect to the substitution of P with Si or S.

of Si or S that can be experimentally incorporated, specifically in  $\text{Na}_x\text{VP}_3$ , remains unclear.<sup>16,38–40</sup>

The physically plausible oxidation states of vanadium in its binary oxides, e.g., VO,  $\text{V}_2\text{O}_3$ ,  $\text{VO}_2$ , and  $\text{V}_2\text{O}_5$ , vary from  $\text{V}^{2+}$  to  $\text{V}^{5+}$ .<sup>55,56</sup> Although the  $\text{V}^{5+}$  state is not observed electrochemically in  $\text{Na}_x\text{VP}_3$ ,<sup>57</sup> it can be accessed in mixed transition metal NaSICON phosphates, such as  $\text{Na}_x\text{VMn}(\text{PO}_4)_3$ ,  $\text{Na}_x\text{VCr}(\text{PO}_4)_3$ , and  $\text{Na}_x\text{NbTi}(\text{PO}_4)_3$ ,<sup>31,58–61</sup> indicating the possibility of its accessibility in mixed polyanion NaSICONs as well. [Figure 2](#) maps the physically accessible regions of Na concentrations and the corresponding V oxidation states at varying contents of  $\text{PO}_4^{3-}$ ,  $\text{SiO}_4^{4-}$ , and  $\text{SO}_4^{2-}$  groups ( $x$ -axis) in the V-based NaSICON framework.

In [Figure 2](#), an increase of  $\text{SiO}_4^{4-}$  concentration in the  $\text{Na}_x\text{VP}_3$  scaffold unsurprisingly favors higher Na concentrations (to compensate for the higher negative charge of  $\text{SiO}_4^{4-}$  groups compared to  $\text{PO}_4^{3-}$ ), whereas the opposite trend is observed with  $\text{SO}_4^{2-}$  substitution. Therefore, the accessible Na content, electrochemically, will decrease from a maximum of 3 in  $\text{Na}_x\text{VP}_3$  ( $\text{Na}_1\text{VP}_3 \leftrightarrow \text{Na}_4\text{VP}_3$ ) to 2 in  $\text{Na}_x\text{VS}_3$  ( $\text{Na}_0\text{VS}_3 \leftrightarrow \text{Na}_2\text{VS}_3$ ) or  $\text{Na}_x\text{VS}_3$  ( $\text{Na}_0\text{VS}_3 \leftrightarrow \text{Na}_2\text{VS}_3$ ), resulting in a decrease in capacity as well. Thus, scenarios where  $\text{PO}_4^{3-}$  is moderately substituted by  $\text{SiO}_4^{4-}$  (or  $\text{SO}_4^{2-}$ ) could provide the maximum possible extractable capacity for Na exchange in the V-based NaSICON system. If Si substitution in  $\text{Na}_3\text{VP}_3$  can enable the extraction of the “last Na ion”, high voltages are to be expected ([Figure 1](#)), which will require appropriate choices (and design) of electrolytes with high anodic stability.<sup>62</sup> Furthermore, for similar substitution levels, the lower weight ([Figure 2](#)) of  $\text{SiO}_4^{4-}$  can slightly increase the gravimetric capacities as compared to  $\text{PO}_4^{3-}$  and  $\text{SO}_4^{2-}$ .

With these hypotheses in mind, we performed DFT calculations to demonstrate the Na (de)intercalation characteristics in  $\text{Na}_x\text{V}_2\text{P}_i(\text{Si/S})_{3-i}\text{O}_{12}$ , where the extent of polyanion mixing varies in the range  $0.0 \leq i \leq 3.0$  in steps of 0.5. For each



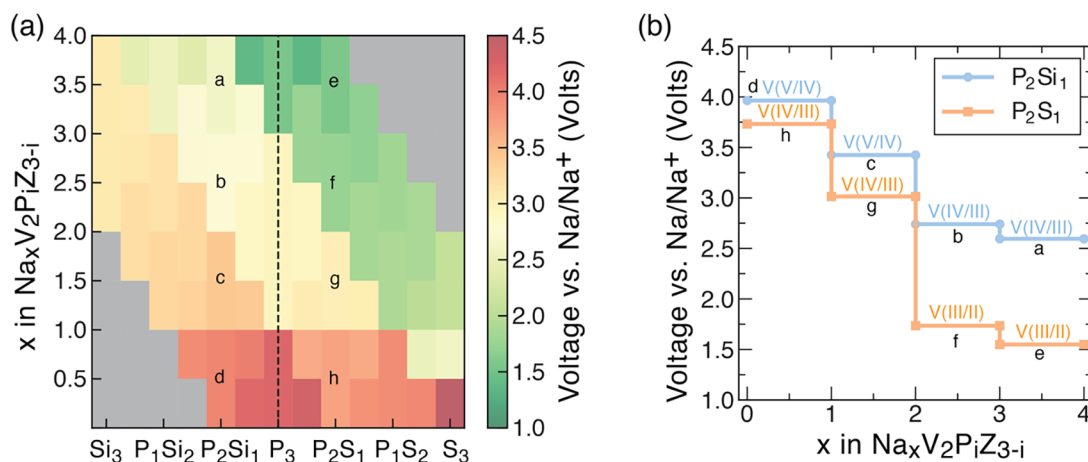


**Figure 3.** a. Map of computed voltage curves (using PBE+U) in mixed  $\text{Na}_x\text{V}_2\text{P}_i(\text{Si/S})_{3-i}\text{O}_{12}$  compounds. The  $x$ -axis represents the polyanion compositions with the degree of mixing given indicated by  $\text{P}_i(\text{Si/S})_{3-i}$  in the  $\text{Na}_x\text{V}_2\text{P}_i(\text{Si/S})_{3-i}\text{O}_{12}$  formula unit, with  $i$  varying in steps of 0.5. The  $y$ -axis represents the Na content per formula unit from  $x = 0$  to  $x = 4$ , also in steps of 0.5. The gray regions correspond to inaccessible vanadium oxidation states, i.e., below  $\text{V}^{2+}$  or above  $\text{V}^{5+}$ . The voltage at each stage of (de)intercalation is indicated by the color bar. b. Calculated voltage curve of selected mixed polyanion compositions of  $\text{P}_2\text{Si}_1$  and  $\text{P}_2\text{S}_1$ . Each voltage step in panel b is labeled and mapped to areas in panel a (via labels a–h).

polyanion composition, we also calculated the Na deintercalation voltages from the change in Na chemical potential as its content is varied within the corresponding NaSICON (see Theoretical Methods section for additional details).

Figure 3a shows the predicted voltages (using PBE+U) as a function of Na (de)intercalation at various substitution levels of  $\text{PO}_4^{3-}$  by  $\text{SiO}_4^{4-}$  or  $\text{SO}_4^{2-}$ . Each column represents a single substitution of  $\text{P}_i(\text{Si/S})_{3-i}$  in  $\text{Na}_x\text{V}_2\text{P}_i(\text{Si/S})_{3-i}\text{O}_{12}$ . The value of each voltage—the color of each box—represents a plateau in the computed voltage curve, similar to those displayed in Figure 1, where each voltage plateau extends over a Na composition range ( $\Delta x$ ) of at least 0.5. Therefore, at a given  $\text{Na}_x\text{V}_2\text{P}_i(\text{Si/S})_{3-i}\text{O}_{12}$ , a change in color moving from a box to another along the  $y$ -axis corresponds to a step in a typical “staircase”-type voltage curve. In general, we observe higher voltages (red boxes) at low Na contents within the NaSICON ( $x < 1$ ) and lower voltages at higher Na contents ( $x > 3$ ). Similarly, large S (Si) substitution at the same Na content tends to decrease (increase) the average voltages, as denoted by the increasing frequency of green (orange) boxes toward the right (left) side of Figure 3a.

To facilitate the reading of Figure 3a, we show the voltage staircase plot for Na (de)intercalation of two selected compositions,  $\text{Na}_x\text{VP}_2\text{Si}_1$  ( $\text{P}_2\text{Si}_1$ ) and  $\text{Na}_x\text{VP}_2\text{S}_1$  ( $\text{P}_2\text{S}_1$ ), in Figure 3b. The two selected mixed polyanion systems display the maximum feasible range of Na (de)intercalation, i.e., the whole  $0 \leq x \leq 4$  range (Figure 2). Note that, at Si/S substitution levels beyond  $\text{P}_2(\text{Si/S})_1$ , the feasible range of Na content in the NaSICON structure reduces since V cannot exhibit stable oxidation states above +5 and below +2. The voltage plateaus in Figure 3b are mapped into Figure 3a through labels from “a” to “h”. Steps at specific Na concentrations in the voltage curves (Figure 3b) correspond to stable compositions in the predicted pseudobinary (i.e., Na-vacancy pseudobinary within  $\text{Na}_x\text{V}_2\text{P}_i(\text{Si/S})_{3-i}\text{O}_{12}$ ) phase diagram.

While the  $\text{V}^{\text{III/II}}$  redox pair is accessed in  $\text{Na}_x\text{VP}_3$  at compositions  $3 < x < 4$ , the  $\text{V}^{\text{III/II}}$  redox couple is not active in  $\text{Na}_x\text{VP}_2\text{Si}_1$  (i.e., 33% substitution of P by Si). Specifically, the  $\text{P}_2\text{Si}_1$  composition involves  $\text{V}^{\text{V/IV}}$  and  $\text{V}^{\text{IV/III}}$  in the regions of  $0 < x < 2$  and  $2 < x < 4$ , respectively, indicating higher average

Na intercalation voltages than those of  $\text{Na}_x\text{VP}_3$  (Figure 1) for similar ranges of Na (de)intercalation. As the  $\text{V}^{\text{IV/III}}$  redox pair can be accessed in both  $\text{Na}_x\text{VP}_3$  ( $1 < x < 3$ ) and  $\text{Na}_x\text{VP}_2\text{Si}_1$  ( $2 < x < 4$ ) by sodium extraction from the Na2 site,<sup>26</sup> the difference in the average voltage of  $\text{V}^{\text{IV/III}}$  for these compounds can be used to accurately determine the effect played by Si on the redox voltage. Specifically, the average voltage of the  $\text{V}^{\text{IV/III}}$  redox for  $\text{Na}_x\text{VP}_2\text{Si}_1$  ( $\sim 2.67$  V vs  $\text{Na/Na}^+$ ,  $(a + b)/2$  in Figure 2) is  $\sim 280$  mV lower than the corresponding voltage for  $\text{Na}_x\text{VP}_3$  ( $\sim 2.95$  V), which can be attributed to the stronger inductive effect of P than of Si.

In  $\text{Na}_x\text{VP}_2\text{Si}_1$ , the step in the voltage curve with Na removal at  $x = 2$  ( $\sim 0.68$  V) is due to the transition from the  $\text{V}^{\text{IV/III}}$  to the  $\text{V}^{\text{V/IV}}$  redox pair. The voltage difference from  $\text{V}^{\text{IV/III}}$  to  $\text{V}^{\text{V/IV}}$  redox in  $\text{Na}_x\text{VP}_2\text{Si}_1$  is almost half of that between the corresponding voltage step for  $\text{Na}_x\text{VP}_3$  ( $\sim 1.33$  V at  $x = 1$ , Figure 1). In  $\text{Na}_1\text{VP}_3$ , the large difference in the voltage steps of the  $\text{V}^{\text{IV/III}}$  to the  $\text{V}^{\text{V/IV}}$  redox is also partly due to the extraction of Na from the Na1 site, pushing the voltage beyond the anodic stability of conventional liquid electrolytes ( $> 4$  V), resulting in the  $\text{V}^{\text{V/IV}}$  redox not being electrochemically accessible.<sup>29</sup> On the other hand, the lower voltage in  $\text{P}_2\text{Si}_1$  may facilitate the extraction of Na from the electrochemically active Na2 site, while the  $\text{V}^{\text{V/IV}}$  redox is active, as indicated by the average voltage of  $\sim 3.42$  V vs  $\text{Na/Na}^+$  for  $1 < x < 2$  (Figure 3b). However, extraction of Na from the Na1 site, which continues to utilize the  $\text{V}^{\text{V/IV}}$  redox in  $\text{P}_2\text{Si}_1$  ( $x < 1$ ), requires a higher voltage ( $\sim 3.96$  V), similar to the observation in  $\text{Na}_x\text{VP}_3$  but marginally within the anodic stability ( $< 4$  V) of conventional liquid electrolytes. The activation of the  $\text{V}^{\text{V/IV}}$  redox and the extraction of Na from the Na1 site in  $\text{P}_2\text{Si}_1$  produces a combined voltage step of  $0.68 + 0.54 = 1.22$  V (i.e., between labels d and b in Figure 3b), which is marginally lower than the  $\sim 1.33$  V jump observed in  $\text{Na}_x\text{VP}_3$ . This difference in the voltage steps between the  $\text{V}^{\text{IV/III}}$  and the  $\text{V}^{\text{V/IV}}$  redox pairs ( $\sim 1.22$  V vs  $\sim 1.33$  V vs  $\text{Na/Na}^+$ ) can also be attributed to the weaker inductive effect in Si than in P.

Overall, our data indicate that the average voltage across the accessible Na concentration ( $0 < x < 4$ ) in  $\text{Na}_x\text{VP}_2\text{Si}_1$  is  $\sim 3.18$  V vs  $\text{Na/Na}^+$ , which is  $\sim 260$  mV higher than the  $\sim 2.92$  V in  $\text{Na}_x\text{VP}_3$ . Thus, the substitution of P by Si facilitates the

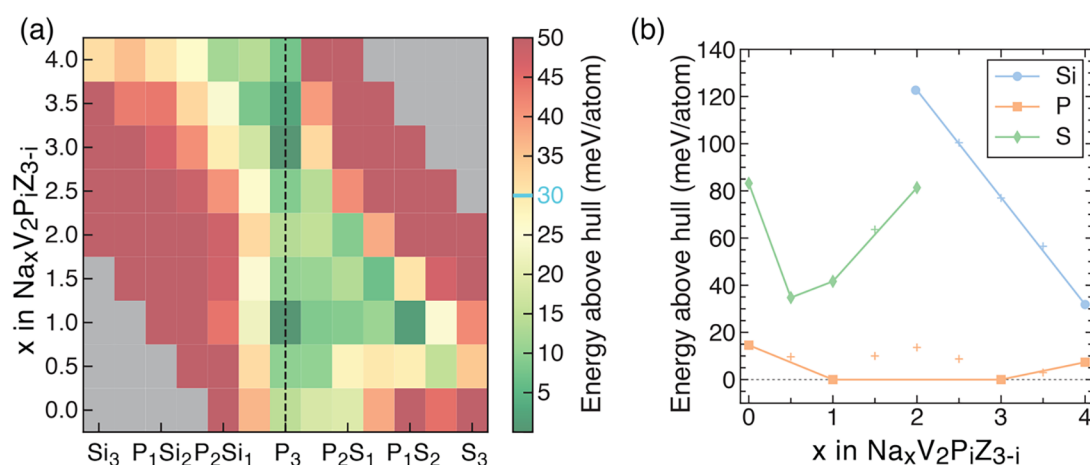


**Figure 4.** a. Stability heatmap in terms of energy above the convex hull (in meV/atom) of mixed polyanion NaSICONs as extracted from the quinary phase diagrams, Na–V–P–Si–O and Na–V–P–S–O. The  $x$  and  $y$  axes are similar to those in Figure 3. The light-blue mark in the color bar represents the limit below which phases are expected to be stabilized by entropic effects and are likely to be synthetically viable. Gray boxes represent areas containing unstable vanadium oxidation states. Instability values higher than 50 meV/atom are also represented by dark red colored boxes. b. Projection of the energies above the hull of selected NaSICON compositions, namely,  $\text{Na}_x\text{VSi}_3$  (light blue),  $\text{Na}_x\text{VP}_3$  (orange), and  $\text{Na}_x\text{VS}_3$  (green), as a function of Na content ( $x$ ).

activation of higher-oxidation-state V redox couples at higher Na concentrations in  $\text{Na}_x\text{VP}_2\text{Si}_1$ , resulting in better intercalation voltages. Si substitution can also result in better capacities than the pure phosphate framework with the possibility of Na extraction from the Na1 site. In our computed (primitive unit cell) model containing 2 formula units of the  $\text{Na}_x\text{VP}_2\text{Si}_1$  framework (total 42 atoms for  $x = 4$ ), the thermodynamically stable ordering is made up of lantern units containing one  $\text{SiO}_4^{4-}$  and two  $\text{PO}_4^{3-}$  tetrahedra, as shown in Figure S2 of the SI. Thus, our model is limited in the number of  $\text{SiO}_4^{4-}$  and  $\text{PO}_4^{3-}$  arrangements enumerated, and this requires more investigation to verify whether other stable Si–P arrangements exist.

In contrast to  $\text{P}_2\text{Si}_1$ , in  $\text{Na}_x\text{VP}_2\text{S}_1$  (33% substitution of P by S) the  $\text{V}^{\text{V/IV}}$  redox pair is not active for  $0 < x < 1$ . Additionally, the  $\text{V}^{\text{IV/III}}$  and  $\text{V}^{\text{III/II}}$  redox couples are active across  $0 < x < 2$  and  $2 < x < 4$ , respectively, in  $\text{P}_2\text{Si}_1$ , while the  $\text{V}^{\text{V/IV}}$  and  $\text{V}^{\text{IV/III}}$  are active for the corresponding Na contents in  $\text{P}_2\text{Si}_1$ , resulting in consistently lower average voltages for the  $\text{P}_2\text{Si}_1$  structures, across all Na concentrations, compared to  $\text{P}_2\text{Si}_1$  (Figure 3b). The stronger inductive effect of  $\text{S}^{6+}$  (vs  $\text{P}^{5+}$  or  $\text{Si}^{4+}$ ) does cause the intercalation voltages to increase for the same active vanadium redox pair. For example, the average voltage of the  $\text{V}^{\text{IV/III}}$  redox couple in  $\text{P}_2\text{S}_1$  is  $\sim 3.37$  V vs  $\text{Na}/\text{Na}^+$  ( $0 < x < 2$ ), which is higher than the  $\sim 2.95$  V in  $\text{Na}_x\text{VP}_3$  ( $1 < x < 3$ ) and  $\sim 2.67$  V in  $\text{P}_2\text{Si}_1$  ( $2 < x < 4$ ). Also, the voltage for  $\text{V}^{\text{IV/III}}$  combined with Na removal from the Na2 site in  $\text{P}_2\text{S}_1$  is  $\sim 3.01$  V vs  $\text{Na}/\text{Na}^+$  ( $1 < x < 2$ ), which is marginally higher than the corresponding voltage ( $\sim 2.95$  V) in  $\text{Na}_x\text{VP}_3$  ( $1 < x < 2$ ). Therefore, S substitution in  $\text{Na}_x\text{VP}$  enhances the voltage of each V redox couple, due to the inductive effect, but reduces the average voltage across the accessible Na concentration via activation of lower-oxidation-state V redox couples.

To assess the synthesizability of Si or S substituted NaSICONs with variable Si/S substitution levels in  $\text{Na}_x\text{VP}_3$ , we have calculated the quinary Na–V–P–Si–O and Na–V–P–S–O phase diagrams (or the 0 K convex hulls) of the  $\text{Na}_x\text{VP}_i(\text{Si/S})_{3-i}$  systems using DFT. The multicomponent phase diagrams provide insight into the thermodynamic stability (at 0 K) of the predicted compositions and constitute

a useful proxy for their synthesizability. The stabilities of each composition of  $\text{Na}_x\text{VP}_{3-i}(\text{Si/S})_i$  are computed with respect to all available elemental, binary, ternary, quaternary, and quinary entities obtained from the Materials Project and the inorganic crystal structure database (ICSD).<sup>63,64</sup> The energies above the convex hull, for compositions considered in steps of  $\Delta x$  and  $\Delta i$  of 0.5, are presented in Figure 4a.

Figure 4b shows the computed energy above the hull as a function of Na content in  $\text{Na}_x\text{VP}_3$  and the fully substituted  $\text{Na}_x\text{VSi}_3$  and  $\text{Na}_x\text{VS}_3$  compositions. Other selected projections of the quinary phase diagrams of Figure 4a are shown in Figure S3 of the SI. Equation S1 in the SI explains how the formation energies and the stabilities of specific  $\text{Na}_x\text{VP}_{3-i}(\text{Si/S})_i$  compounds are assessed.

If we qualitatively assume that  $\sim 30$  meV/atom is the (vibrational) entropic stabilization accessible at room temperature (see the blue line in the color bar of Figure 4a),<sup>65–67</sup> our results suggest that only NaSICONs with low Si ( $0 < i < 0.5$ ) and low S ( $0 < i < 1$ ) contents might be experimentally accessible for specific ranges of Na concentrations.

Furthermore, the fully substituted  $\text{Na}_x\text{VSi}_3$  and  $\text{Na}_x\text{VS}_3$  display large instabilities ( $>30$  meV/atom), as seen in Figure 4a,b, suggesting difficulties in their experimental synthesis. To elaborate further, the convex hull of quaternary  $\text{Na}_x\text{VP}_3$  (orange line in Figure 4b) shows that only  $\text{Na}_x\text{VP}_3$  structures at  $x = 1$  and  $x = 3$  are stable, with  $x = 4$  and  $x = 0$  being metastable ( $\sim 7.3$  and  $\sim 14.6$  meV/atom) at 0 K, respectively. This is in qualitative agreement with experimental reports that use  $\text{Na}_3\text{VP}$  to form  $\text{Na}_1\text{VP}_3$  and  $\text{Na}_4\text{VP}_3$  via electrochemical extraction/insertion.<sup>31,33</sup> Although the fully deintercalated  $\text{Na}_0\text{VP}_3$  shows only marginal instability ( $\sim 14.6$  meV/atom with the decomposition products of  $\text{VP}_2\text{O}_7$  and  $\text{VPO}_5$ ), it is not electrochemically accessible.<sup>24</sup>

In the case of  $\text{Na}_4\text{VSi}_3$ , we predict that the NaSICON phase will decompose into stable  $\text{NaV}(\text{SiO}_3)_2$ ,  $\text{Na}_2\text{Si}_2\text{O}_5$ ,  $\text{NaVO}_3$ , and  $\text{Na}_3\text{VO}_4$ , where the decomposition involves disproportionation of V from its 4+ oxidation state in NaSICON to 3+ in  $\text{NaV}(\text{SiO}_3)_2$  and 5+ in  $\text{NaVO}_3$  and  $\text{Na}_3\text{VO}_4$ . The corresponding desodiated composition  $\text{Na}_2\text{VSi}_3$  (with  $\text{V}^{5+}$ ) decomposes into  $\text{NaVO}_3$  and  $\text{SiO}_2$ . The NaSICON with a low

concentration of Si, i.e.,  $\text{Na}_x\text{VP}_{2.5}\text{Si}_{0.5}$ , shows low instabilities (7–32 meV/atom) across the whole range of Na concentrations  $0 \leq x \leq 4$ , indicating that low Si substitution may be accessible at room temperature. However, we do not expect higher Si content ( $i > 0.5$ ) in  $\text{Na}_x\text{VP}_{3-i}\text{Si}_i$  to be favorable for synthesis. Additionally, the minimum energy configurations (i.e., most negative formation energies with respect to elements or the lowest energy above convex hull values) shift from  $x = 3$  in  $\text{Na}_3\text{VP}_3$  to higher Na contents,  $x = 3.5$  and  $4$ , when a fraction of Si ( $i = 0.5$  and  $1$ , respectively) substitutes for P. In general, compositions with Na contents between  $x = 1$  and  $3.5$  remain metastable ( $<30$  meV/atom) with small Si addition (up to  $i = 0.5$ ), which may be accessible via high temperature synthesis.

In the case of S substitution, we predict that the NaSICON– $\text{Na}_2\text{VS}_3$  will decompose into stable  $\text{Na}_2\text{SO}_4$ ,  $\text{SO}_2$ , and  $\text{VO}_2$ , with oxidation of V from its 2+ oxidation state in NaSICON to 4+ in  $\text{VO}_2$  accompanied by a reduction of  $\text{S}^{6+}$  in NaSICON to 4+ in  $\text{SO}_2$ . The corresponding desodiated composition  $\text{Na}_0\text{VS}_3$  (with  $\text{V}^{\text{III}}$ ) decomposes into  $\text{VO}_2$  ( $\text{V}^{\text{IV}}$ ),  $\text{SO}_3$  ( $\text{S}^{6+}$ ), and  $\text{SO}_2$  ( $\text{S}^{4+}$ ). In contrast to Si, the substitution of P by S shifts the minimum energy configurations to lower Na content (green boxes in Figure 4a). Specifically, Na concentrations near  $x = 1$  become energetically favorable (i.e., low instabilities) with increasing S content. Hence, S substitution will favor synthesizing NaSICONs with lower Na content compared to the pure phosphate or Si substituted versions. Nevertheless, large S substitutions ( $i > 1$ ) result in high instabilities ( $>30$  meV/atom) at most Na contents within the NaSICON, indicating synthesis difficulties and possible decomposition during electrochemical experiments.

#### 4. DISCUSSION

$\text{PO}_4^{3-}$  substitution by  $\text{SiO}_4^{4-}$  or  $\text{SO}_4^{2-}$  in  $\text{Na}_x\text{VP}_3$  modifies the redox voltages of the feasible V redox pairs, namely,  $\text{V}^{\text{III/II}}$ ,  $\text{V}^{\text{IV/III}}$ , and  $\text{V}^{\text{V/IV}}$ . Due to the lower oxidation state of Si than P, the presence of Si decreases the average voltage of each V redox couple, while S shows the opposite trend (Figure 3). This behavior can be attributed to a progressive increase in inductive effect, in the order  $\text{Si} < \text{P} < \text{S}$ . However, with Si and S introduction into  $\text{Na}_x\text{VP}$ , the shifts in the overall average voltages arise from the activation of the high voltage  $\text{V}^{\text{V/IV}}$  redox pairs in the case of Si (resulting in overall higher average voltage than P) and the low voltage  $\text{V}^{\text{III/II}}$  redox pairs in S (lower overall average voltage). Importantly, the high voltage  $\text{V}^{\text{V/IV}}$  redox can be accessed with Si substitution even without extraction from the Na1 site, which is not feasible in the parent  $\text{Na}_x\text{VP}_3$  structure.<sup>26</sup> From our predictions, Si substitution appears to decouple the voltage required for the  $\text{V}^{\text{V/IV}}$  redox and the activation of the Na1 site (labels c and d in Figure 3), making the  $\text{V}^{\text{V/IV}}$  couple accessible within the practical stability windows of conventional electrolytes.

It is important to discuss the effects of vibrational and configurational entropy contributions in favoring the synthesizability of potential mixed  $\text{Na}_x\text{VP}_{3-i}(\text{Si/S})_i$  compositions. First, there cannot be a general criterion suggesting that any arbitrary phase will be stabilized by some amount vibrational entropy with respect to other competing phases. The entropic (vibrational) stabilization depends critically on how the target NaSICON composition of interest responds to temperature effects relative to all relevant competing phases for that target compound. The second important thermodynamic handle that controls the formation of mixed  $\text{Na}_x\text{VP}_{3-i}(\text{Si/S})_i$  compositions

is the configurational entropy arising from both Na/vacancies and/or Si/P (or S/P) mixing. Previously, we have elucidated the role of configurational entropy linked to the Na/vacancy lattice in  $\text{Na}_x\text{VP}_3$ ,<sup>26</sup> whose magnitude for compositions between  $\text{Na}_1\text{VP}_3$  and  $\text{Na}_3\text{VP}_3$  appears negligible ( $\sim 1$  J/K). This low value of configurational entropy is the result of the significant stability of specific Na/vacancy orderings at  $\text{Na}_1\text{VP}_3$  and  $\text{Na}_3\text{VP}_3$ ,<sup>26,29</sup> which competes with the configurational entropy from the Si(S) mixing with P in  $\text{Na}_x\text{VP}_{3-i}(\text{Si/S})_i$ . Here, using a simple model of ideal solution shown in Figure 5,

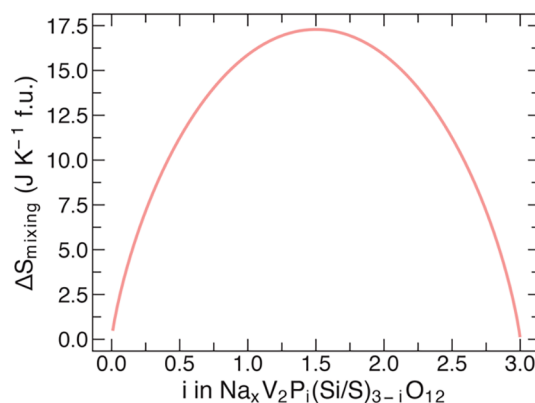


**Figure 5.** Estimated configurational entropy arising from Si(S) in  $\text{Na}_x\text{VP}_3$ . The ideal solution model  $\Delta S_{\text{mixing}} = -nR[i \times \ln(i)] + [(1-i) \times \ln(1-i)]$  was used, where  $n$  is the number of P atoms per f.u.,  $R$  is the molar gas constant, and  $i$  is the amount of either Si or S mixed with P in  $\text{Na}_x\text{VP}_3$ .

we have estimated that the entropy stabilization from the Si/P (or S/P) mixing in  $\text{Na}_x\text{V}_2(\text{PO}_4)_3$  reaches a maximum at  $i = 1.5$  Si (S) in  $\text{Na}_x\text{VP}_{3-i}(\text{Si/S})_i$  of  $\sim 17$  J K<sup>−1</sup>. This finding demonstrates that Si/P or S/P mixing may favor the synthesis of these mixed NaSICON phases.

Indeed, the replacement of phosphate groups ( $\text{PO}_4^{3-}$ ) by silicate groups ( $\text{SiO}_4^{4-}$ ) in  $\text{Na}_3\text{VP}_3$  to prepare the Na-rich  $\text{Na}_{3+i}\text{VP}_{3-i}\text{Si}_i$  (with  $i = 0.1, 0.2$ , and  $0.4$ ) solid solutions has been reported by Aragón et al.<sup>39</sup> and more recently reinvestigated by Pal et al.<sup>16</sup> The composition  $\text{Na}_{3.4}\text{VP}_{2.6}\text{Si}_{0.4}$  included a large fraction of impurities that could not be assigned by the authors.<sup>16,39</sup> Although our phase diagram in Figure 4 suggests that the Na-rich/Si-rich  $\text{Na}_{3.5}\text{VP}_{2.5}\text{Si}_{0.5}$  is slightly metastable, it tends to decompose into the  $\text{Na}_3\text{V}(\text{PO}_4)_2$ ,  $\text{V}_2\text{O}_3$ ,  $\text{NaV}(\text{SiO}_3)_2$ , and  $\text{Na}_3\text{V}_2(\text{PO}_4)_3$  phases, which may have been the impurities in the synthesized  $\text{Na}_{3.4}\text{VP}_{2.6}\text{Si}_{0.4}$ .<sup>16</sup> Thus, more experimental studies are required to ascertain the extent of solubility of Si in  $\text{Na}_x\text{VP}_3$ . While a moderate capacity increase was reported for  $\text{Na}_{3.1}\text{VP}_{2.9}\text{Si}_{0.1}$  (first discharge  $\sim 100$  mAh/g at C/10) and  $\text{Na}_{3.2}\text{VP}_{2.8}\text{Si}_{0.2}$  (first discharge  $\sim 98$  mAh/g at C/10) in comparison to  $\text{Na}_3\text{VP}_3$  ( $\sim 88$  mAh/g at C/10),<sup>16</sup> the authors did not explore the high-voltage domain of the  $\text{V}^{\text{V/IV}}$  redox couple in the Si-substituted NaSICONs.

The predicted average voltage (vs  $\text{Na}/\text{Na}^+$ ) for  $\text{Na}_x\text{VP}_{3-i}(\text{Si/S})_i$  compounds together with the corresponding theoretical gravimetric capacities provide the theoretical energy densities (see Figure S4). At lower Si or S substitutions for P ( $i < 0.5$ ), as the accessible Na concentrations range remains unchanged for all the compositions (i.e.,  $1 < x < 4$ ), the negligible difference in the gravimetric capacities only arises from the small differences in the masses of Si and S.



Additionally, a high degree of substitution of either Si or S ( $i > 1$ ) for P significantly reduces the gravimetric capacity, and the energy density, due to the reduction in the feasible range for Na extraction per formula unit. Furthermore, our stability predictions (Figure 4) also point to increasing synthesis difficulties upon high degrees of Si/S substitution ( $i > 1$ ) in  $\text{Na}_x\text{VP}_{3-i}(\text{Si/S})_i$ .

Although the Na-intercalation voltage for each V redox couple increases with S substitution compared to Si due to the enhanced inductive effect of S, the average voltage for deintercalation, across the accessible Na range, is higher with Si substitution than with S. For example, a small degree of S substitution in  $\text{Na}_x\text{VP}_3$  extends the activity of the low voltage  $\text{V}^{\text{III/II}}$  redox pair over a larger Na content range, thereby reducing the overall average voltage. On the other hand, a small amount of Si extends the high voltage  $\text{V}^{\text{V/IV}}$  redox couple over a larger Na content range, thereby improving the overall average and the theoretical energy density. Thus, an improvement in the gravimetric capacity combined with the overall higher voltage through activation of the  $\text{V}^{\text{V/IV}}$  redox couple achieved by  $\text{Na}_x\text{VP}_{3-i}\text{Si}_i$  (at  $i < 1$ ) offers an opportunity to increase the energy density of Na batteries that employ NaSICON electrodes. Furthermore, the replacement of  $\text{P}^{5+}$  by  $\text{Si}^{4+}$  may reduce the barriers for Na migration in NaSICON electrodes due to reduced electrostatic repulsions between migration of  $\text{Na}^+$  and Z cations.

## 5. CONCLUSIONS

In summary, by using DFT calculations combined with a robust thermodynamic analysis, we have explored the effect of polyanionic substitution on the structure, stability, and electrochemical behavior of the vanadium-based NaSICON,  $\text{Na}_x\text{V}_2(\text{PO}_4)_3$ . Although  $\text{PO}_4^{3-}$  substitution with  $\text{SO}_4^{2-}$  enhances the voltage of each V redox, it lowers the overall average voltage due to the extension of the low voltage  $\text{V}^{\text{III/II}}$  redox couple. In contrast,  $\text{SiO}_4^{4-}$  substitution is found to activate the high voltage  $\text{V}^{\text{V/IV}}$  redox couple without necessarily removing Na from the Na1 site, resulting in a higher overall average voltage. Note that activating the  $\text{V}^{\text{V/IV}}$  redox couple without Na extraction from the Na1 site is not possible in the parent  $\text{Na}_x\text{VP}_3$  compound. The computed quinary phase diagrams of  $\text{Na-V-P-(Si/S)-O}$  indicate that small degrees of Si/S substitution should be experimentally feasible. Our computed theoretical energy densities highlight that incorporating low Si contents into  $\text{Na}_x\text{VP}_3$  appears a feasible pathway for improving the energy densities of NaSICON cathodes.

## 6. THEORETICAL METHODS

To determine the effect of Si and S substitution at the P site of  $\text{Na}_x\text{VP}_3$ , structures of  $\text{Na}_x\text{VP}_{3-i}(\text{Si/S})_i\text{O}_{12}$  with  $i$  ranging from 0 to 3 at step sizes of 0.5 were examined, providing  $\text{Na}_x\text{V}_2(\text{PO}_4)_3$  ( $i = 0, \text{P}_3$ ),  $\text{Na}_x\text{V}_2\text{P}_{2.5}(\text{Si/S})_{0.5}\text{O}_{12}$  ( $i = 0.5, \text{P}_{2.5}(\text{Si/S})_{0.5}$ ),  $\text{Na}_x\text{V}_2\text{P}_2(\text{Si/S})_1\text{O}_{12}$  ( $i = 1.0, \text{P}_2(\text{Si/S})_1$ ),  $\text{Na}_x\text{V}_2\text{P}_{1.5}(\text{Si/S})_{1.5}\text{O}_{12}$  ( $i = 1.5, \text{P}_{1.5}(\text{Si/S})_{1.5}$ ),  $\text{Na}_x\text{V}_2\text{P}_1(\text{Si/S})_2\text{O}_{12}$  ( $i = 2, \text{P}_1(\text{Si/S})_2$ ),  $\text{Na}_x\text{V}_2\text{P}_{0.5}(\text{Si/S})_{2.5}\text{O}_{12}$  ( $i = 2.5, \text{P}_{0.5}(\text{Si/S})_{2.5}$ ), and  $\text{Na}_x\text{V}_2(\text{Si/S})_3\text{O}_{12}$  ( $i = 3, (\text{Si/S})_3$ ), respectively. These compositions were studied with Na content  $x$  ranging from 0 to 4 with step sizes of 0.5 for  $x$ . Thus, the concentration steps of 0.5 along the  $i$  and  $x$  variables result in a total of 97 distinct compositions (number of nongray squares

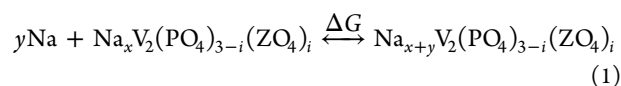
in Figures 3 and 4). Fully Na ordered  $\text{Na}_4\text{VP}_{3-i}(\text{Si/S})_i$  structures were generated from a reference structure of the NaSICON, namely, the rhombohedral ( $R\bar{3}c$ ) primitive cell containing 2 formula units per unit cell found in the ICSD database (id: 20340).<sup>64</sup>

In this primitive structure, Si and S were partially (or fully) substituted onto P sites, and Na atoms were extracted to generate new configurations of  $\text{Na}_x\text{VP}_{3-i}(\text{Si/S})_i$  at different Na contents. Various Na/vacancy and Si/P (S/P) orderings were enumerated using the pymatgen package.<sup>68</sup> To minimize the number of orderings, we used a ranking scheme based on the Ewald energy,<sup>69</sup> where the electrostatic energy was computed after assigning integer point charges to each species ( $\text{Na} = +1$ ,  $\text{Si} = +4$ ,  $\text{P} = +5$ ,  $\text{S} = +6$ , and  $\text{O} = -2$ , V charges assigned based on Na and Si/S content).<sup>69</sup> At each Na composition, 500 structures with the lowest Ewald energies were selected. The final number of structures computed was further reduced by symmetry considerations.

To ascertain the thermodynamic stability of the mixed polyanion phases, we computed the quinary phase diagrams. This implies that all known and ordered binary, ternary, quaternary, and quinary compounds for the  $\text{Na-V-P-Si-O}$  and  $\text{Na-V-P-S-O}$  systems found in the ICSD were calculated (apart from the pure elements) and complemented by structures available in the Materials Project.<sup>63,64</sup>

The Vienna ab initio simulation package (version 5.4.4) software was used to perform DFT total energy calculations of the structures considered. The wave functions were described by planewaves extending to a maximum kinetic energy of 520 eV, which was combined with projector augmented wave (PAW) potentials for core electrons. The PAW potentials used were Na 08Apr2002 3s<sup>1</sup>, V\_pv 07Sep2000 3p<sup>6</sup>3d<sup>4</sup>4s<sup>1</sup>, P 17Jan2003 3s<sup>2</sup>3p<sup>3</sup>, Si 05Jan2001 3s<sup>2</sup>3p<sup>2</sup>, S 17Jan2003 3s<sup>2</sup>3p<sup>4</sup>, and O 08Apr2002 2s<sup>2</sup>2p<sup>4</sup>. PBE-parametrized spin-polarized generalized gradient approximation (GGA) was used for the exchange and correlation energy, and the Dudarev method was introduced to account for the on-site Coulomb repulsions between 3d electrons of vanadium,<sup>70</sup> by incorporating a Hubbard  $U$  parameter of 3.1 eV.<sup>50</sup> The  $U$  parameter has been derived for oxide compounds, and it may be less accurate for polyanion compounds, as in this study. Hence, we also performed test calculations with the screened hybrid functional, HSE06.<sup>49,71</sup> The irreducible Brillouin zone was sampled using a  $\Gamma$ -point-centered Monkhorst–Pack mesh with a minimum of 25 subdivisions along each reciprocal lattice vector. The total energies were considered converged when differences were less than 10<sup>−5</sup> eV/structure, forces on atom less than 10<sup>−2</sup> eV/Å, and stresses less than 0.29 GPa.

**6.1. Calculation of Voltages for Na Extraction.** The reversible extraction of Na ions from the NaSICON  $\text{Na}_x\text{VP}_{3-i}(\text{Si/S})_i$  framework can provide an intercalation battery according to the redox reaction of eq 1.



The DFT total energy was used to approximate the Gibbs energy,  $G$ , of each compound in eq 1, and the average voltage  $\langle V \rangle$  at each stage of intercalation is calculated following eq 2, with  $F$  being the Faraday constant.<sup>72</sup>

$$\langle V \rangle = \frac{-\Delta G}{yF} = \frac{E[\text{Na}_{x+y}\text{V}_2(\text{PO}_4)_{3-i}(\text{ZO}_4)_i] - yE[\text{Na}] - yE[\text{Na}_x\text{V}_2(\text{PO}_4)_{3-i}(\text{ZO}_4)_i]}{yF} \quad (2)$$

In this approximation both the entropic contribution and the  $pV$  terms are neglected.

## ■ ASSOCIATED CONTENT

### Supporting Information

The Supporting Information is available free of charge at <https://pubs.acs.org/doi/10.1021/acs.chemmater.2c00230>.

Theoretical framework to develop the NaSICON phase diagrams, phase diagrams of NaSICON  $\text{Na}_x\text{V}_2(\text{PO}_4)_3$  and  $\text{Na}_x\text{V}_2\text{P}_{i-1}\text{Si}_{3-i}\text{O}_{12}$ , decomposition reactions of NaSICON  $\text{Na}_x\text{V}_2\text{P}_{i-1}\text{Si}_{3-i}\text{O}_{12}$ , and models of  $\text{Na}_x\text{V}_2\text{P}_2\text{Si}_1\text{O}_{12}$  (PDF)

## ■ AUTHOR INFORMATION

### Corresponding Author

**Pieremanuele Canepa** – Department of Materials Science and Engineering, National University of Singapore, Singapore 117575; Chemical and Biomolecular Engineering, National University of Singapore, Singapore 117585; [orcid.org/0000-0002-5168-9253](https://orcid.org/0000-0002-5168-9253); Email: [pcanepa@nus.edu.sg](mailto:pcanepa@nus.edu.sg)

### Authors

**Vishakha Kapoor** – Department of Materials Science and Engineering, National University of Singapore, Singapore 117575

**Baltej Singh** – Department of Materials Science and Engineering, National University of Singapore, Singapore 117575

**Gopalakrishnan Sai Gautam** – Department of Materials Engineering, Indian Institute of Science, Bengaluru 560012 Karnataka, India; [orcid.org/0000-0002-1303-0976](https://orcid.org/0000-0002-1303-0976)

**Anthony K. Cheetham** – Department of Materials Science and Engineering, National University of Singapore, Singapore 117575; Materials Department and Materials Research Laboratory, University of California, Santa Barbara, California 93106, United States; [orcid.org/0000-0003-1518-4845](https://orcid.org/0000-0003-1518-4845)

Complete contact information is available at: <https://pubs.acs.org/doi/10.1021/acs.chemmater.2c00230>

### Author Contributions

#(V.K. and B.S.) These authors contributed equally.

### Notes

The authors declare no competing financial interest.

## ■ ACKNOWLEDGMENTS

P.C. and A.K.C. are grateful for the ANR-NRF NRF2019-NRF-ANR073 Na-MASTER. P.C. and B.S. acknowledge funding from the National Research Foundation under the NRF Fellowship NRFF12-2020-0012. A.K.C. thanks the Ras Al Khaimah Center for Advanced Materials for financial support. The computational work was performed using resources of the National Supercomputing Centre, Singapore (<https://www.nssc.sg>).

## ■ REFERENCES

- (1) U.S. Geological Survey data release. *Lithium*; Mineral Commodities Summaries; 2021.
- (2) Tarascon, J.-M. Is Lithium the New Gold? *Nat. Chem.* **2010**, *2* (6), 510–511.
- (3) Olivetti, E. A.; Ceder, G.; Gaustad, G. G.; Fu, X. Lithium-Ion Battery Supply Chain Considerations: Analysis of Potential Bottlenecks in Critical Metals. *Joule* **2017**, *1* (2), 229–243.
- (4) Larcher, D.; Tarascon, J.-M. Towards Greener and More Sustainable Batteries for Electrical Energy Storage. *Nat. Chem.* **2015**, *7* (1), 19–29.
- (5) Slater, M. D.; Kim, D.; Lee, E.; Johnson, C. S. Sodium-Ion Batteries. *Adv. Funct. Mater.* **2013**, *23* (8), 947–958.
- (6) Delmas, C. Sodium and Sodium-Ion Batteries: 50 Years of Research. *Adv. Energy Mater.* **2018**, *8* (17), 1703137.
- (7) Jian, Z.; Hu, Y.-S.; Ji, X.; Chen, W. NASICON-Structured Materials for Energy Storage. *Adv. Mater.* **2017**, *29* (20), 1601925.
- (8) Goodenough, J. B.; Hong, H. Y.-P.; Kafalas, J. A. Fast Na<sup>+</sup>-Ion Transport in Skeleton Structures. *Mater. Res. Bull.* **1976**, *11* (2), 203–220.
- (9) Kim, S.-W.; Seo, D.-H.; Ma, X.; Ceder, G.; Kang, K. Electrode Materials for Rechargeable Sodium-Ion Batteries: Potential Alternatives to Current Lithium-Ion Batteries. *Adv. Energy Mater.* **2012**, *2* (7), 710–721.
- (10) Bai, Q.; Yang, L.; Chen, H.; Mo, Y. Computational Studies of Electrode Materials in Sodium-Ion Batteries. *Adv. Energy Mater.* **2018**, *8* (17), 1702998.
- (11) Hasa, I.; Mariyappan, S.; Saurel, D.; Adelhelm, P.; Kopolov, A. Y.; Masquelier, C.; Croguennec, L.; Casas-Cabanas, M. Challenges of Today for Na-Based Batteries of the Future: From Materials to Cell Metrics. *J. Power Sources* **2021**, *482*, 228872.
- (12) Wang, P.-F.; You, Y.; Yin, Y.-X.; Guo, Y.-G. Layered Oxide Cathodes for Sodium-Ion Batteries: Phase Transition, Air Stability, and Performance. *Adv. Energy Mater.* **2018**, *8* (8), 1701912.
- (13) Padhi, A. K.; Manivannan, V.; Goodenough, J. B. Tuning the Position of the Redox Couples in Materials with NASICON Structure by Anionic Substitution. *J. Electrochem. Soc.* **1998**, *145* (5), 1518–1520.
- (14) Masquelier, C.; Croguennec, L. Polyanionic (Phosphates, Silicates, Sulfates) Frameworks as Electrode Materials for Rechargeable Li (or Na) Batteries. *Chem. Rev.* **2013**, *113* (8), 6552–6591.
- (15) Jin, T.; Li, H.; Zhu, K.; Wang, P.-F.; Liu, P.; Jiao, L. Polyanion-Type Cathode Materials for Sodium-Ion Batteries. *Chem. Soc. Rev.* **2020**, *49* (8), 2342–2377.
- (16) Pal, S. K.; Thirupathi, R.; Chakrabarty, S.; Omar, S. Improving the Electrochemical Performance of  $\text{Na}_3\text{V}_2(\text{PO}_4)_3$  Cathode in Na-Ion Batteries by Si-Doping. *ACS Appl. Energy Mater.* **2020**, *3* (12), 12054–12065.
- (17) Nanjundaswamy, K. Synthesis, Redox Potential Evaluation and Electrochemical Characteristics of NASICON-Related-3D Framework Compounds. *Solid State Ion* **1996**, *92* (1–2), 1–10.
- (18) Padhi, A. K.; Nanjundaswamy, K. S.; Masquelier, C.; Goodenough, J. B. Mapping of Transition Metal Redox Energies in Phosphates with NASICON Structure by Lithium Intercalation. *J. Electrochem. Soc.* **1997**, *144* (8), 2581–2586.
- (19) Manthiram, A. A Reflection on Lithium-Ion Battery Cathode Chemistry. *Nat. Commun.* **2020**, *11* (1), 1550.
- (20) Kim, H.; Kim, H.; Ding, Z.; Lee, M. H.; Lim, K.; Yoon, G.; Kang, K. Recent Progress in Electrode Materials for Sodium-Ion Batteries. *Adv. Energy Mater.* **2016**, *6* (19), 1600943.
- (21) Ni, Q.; Bai, Y.; Wu, F.; Wu, C. Polyanion-Type Electrode Materials for Sodium-Ion Batteries. *Adv. Sci.* **2017**, *4* (3), 1600275.



- (22) Barpanda, P.; Oyama, G.; Nishimura, S.; Chung, S.-C.; Yamada, A. A 3.8-V Earth-Abundant Sodium Battery Electrode. *Nat. Commun.* **2014**, *5* (1), 4358.
- (23) Hong, H. Y.-P. Lincoln Laboratory. Crystal Structures and Crystal Chemistry in the System  $\text{NaI}+\text{xZr}_2\text{SixP}_3\text{O}_{12}$ . *Mater. Res. Bull.* **1976**, *11*, 173–182.
- (24) Singh, B.; Wang, Z.; Park, S.; Gautam, G. S.; Chotard, J.-N.; Croguennec, L.; Carlier, D.; Cheetham, A. K.; Masquelier, C.; Canepa, P. A Chemical Map of NaSICON Electrode Materials for Sodium-Ion Batteries. *J. Mater. Chem. A* **2021**, *9* (1), 281–292.
- (25) Park, S.; Chotard, J.-N.; Carlier, D.; Moog, I.; Courty, M.; Duttine, M.; Fauth, F.; Iadecola, A.; Croguennec, L.; Masquelier, C. Crystal Structures and Local Environments of NASICON-Type  $\text{Na}_3\text{FeV}(\text{PO}_4)_3$  and  $\text{Na}_4\text{FeV}(\text{PO}_4)_3$  Positive Electrode Materials for Na-Ion Batteries. *Chem. Mater.* **2021**, *33* (13), 5355–5367.
- (26) Wang, Z.; Park, S.; Deng, Z.; Carlier, D.; Chotard, J.-N.; Croguennec, L.; Gautam, G. S.; Cheetham, A. K.; Masquelier, C.; Canepa, P. Phase Stability and Sodium-Vacancy Orderings in a NaSICON Electrode. *J. Mater. Chem. A* **2021**, *10* (1), 209–217.
- (27) Kawai, K.; Asakura, D.; Nishimura, S.; Yamada, A. Stabilization of a 4.5 V  $\text{Cr}^{4+}/\text{Cr}^{3+}$  Redox Reaction in NASICON-Type  $\text{Na}_3\text{Cr}_2(\text{PO}_4)_3$  by Ti Substitution. *Chem. Commun.* **2019**, 55 (91), 13717–13720.
- (28) Ouyang, B.; Wang, J.; He, T.; Bartel, C. J.; Huo, H.; Wang, Y.; Lacivita, V.; Kim, H.; Ceder, G. Synthetic Accessibility and Stability Rules of NASICONs. *Nat. Commun.* **2021**, *12* (1), 5752.
- (29) Park, S.; Wang, Z.; Deng, Z.; Moog, I.; Canepa, P.; Fauth, F.; Carlier, D.; Croguennec, L.; Masquelier, C.; Chotard, J.-N. Crystal Structure of  $\text{Na}_2\text{V}_2(\text{PO}_4)_3$ , an Intriguing Phase Spotted in the  $\text{Na}_3\text{V}_2(\text{PO}_4)_3$ - $\text{Na}_1\text{V}_2(\text{PO}_4)_3$  System. *Chem. Mater.* **2022**, *34*, 451.
- (30) Barim, G.; Cottingham, P.; Zhou, S.; Melot, B. C.; Brutchey, R. L. Investigating the Mechanism of Reversible Lithium Insertion into Anti-NASICON  $\text{Fe}_2(\text{WO}_4)_3$ . *ACS Appl. Mater. Interfaces* **2017**, *9* (12), 10813–10819.
- (31) Lalère, F.; Seznec, V.; Courty, M.; David, R.; Chotard, J. N.; Masquelier, C. Improving the Energy Density of  $\text{Na}_3\text{V}_2(\text{PO}_4)_3$ -Based Positive Electrodes through V/Al Substitution. *J. Mater. Chem. A* **2015**, *3* (31), 16198–16205.
- (32) Yao, X.; Zhu, Z.; Li, Q.; Wang, X.; Xu, X.; Meng, J.; Ren, W.; Zhang, X.; Huang, Y.; Mai, L. 3.0 V High Energy Density Symmetric Sodium-Ion Battery:  $\text{Na}_4\text{V}_2(\text{PO}_4)_3\|\text{Na}_3\text{V}_2(\text{PO}_4)_3$ . *ACS Appl. Mater. Interfaces* **2018**, *10* (12), 10022–10028.
- (33) Ishado, Y.; Inoishi, A.; Okada, S. Exploring Factors Limiting Three- $\text{Na}^+$  Extraction from  $\text{Na}_3\text{V}_2(\text{PO}_4)_3$ . *Electrochemistry* **2020**, *88* (5), 457–462.
- (34) Lalère, F.; Leriche, J. B.; Courty, M.; Boulineau, S.; Viallet, V.; Masquelier, C.; Seznec, V. An All-Solid State NASICON Sodium Battery Operating at 200 °C. *J. Power Sources* **2014**, *247*, 975–980.
- (35) Noguchi, Y.; Kobayashi, E.; Plashnitsa, L. S.; Okada, S.; Yamaki, J. Fabrication and Performances of All Solid-State Symmetric Sodium Battery Based on NASICON-Related Compounds. *Electrochim. Acta* **2013**, *101*, 59–65.
- (36) Plashnitsa, L. S.; Kobayashi, E.; Noguchi, Y.; Okada, S.; Yamaki, J. Performance of NASICON Symmetric Cell with Ionic Liquid Electrolyte. *J. Electrochem. Soc.* **2010**, *157* (4), A536.
- (37) Padhi, A. K.; Manivannan, V.; Goodenough, J. B. Tuning the Position of the Redox Couples in Materials with NASICON Structure by Anionic Substitution. *J. Electrochem. Soc.* **1998**, *145* (5), 1518–1520.
- (38) Chen, Y.; Cheng, J.; He, Z.; Wang, Y.; Wang, C.; Guo, L. Silicon Substituted  $\text{Na}_3\text{V}_2(\text{PO}_4)_3/\text{C}$  Nanocomposites Enwrapped on Conducting Graphene for High-Rate and Long-Lifespan Sodium Ion Batteries. *Ceram. Int.* **2020**, *46* (17), 27660–27669.
- (39) Aragón, M. J.; Lavela, P.; Ortiz, G. F.; Alcántara, R.; Tirado, J. L. On the Effect of Silicon Substitution in  $\text{Na}_3\text{V}_2(\text{PO}_4)_3$  on the Electrochemical Behavior as Cathode for Sodium-Ion Batteries. *ChemElectroChem* **2018**, *5* (2), 367–374.
- (40) Cheng, J.; Chen, Y.; Wang, Y.; Wang, C.; He, Z.; Li, D.; Guo, L. Insights into the Enhanced Sodium Storage Property and Kinetics Based on the Zr/Si Codoped  $\text{Na}_3\text{V}_2(\text{PO}_4)_3/\text{C}$  Cathode with Superior Rate Capability and Long Lifespan. *J. Power Sources* **2020**, *474*, 228632.
- (41) Wang, M.; Guo, J.; Wang, Z.; Gu, Z.; Nie, X.; Yang, X.; Wu, X. Isostructural and Multivalent Anion Substitution toward Improved Phosphate Cathode Materials for Sodium-Ion Batteries. *Small* **2020**, *16* (16), 1907645.
- (42) Kohn, W.; Sham, L. J. Self-Consistent Equations Including Exchange and Correlation Effects. *Phys. Rev.* **1965**, *140* (4A), A1133–A1138.
- (43) Hohenberg, P.; Kohn, W. Inhomogeneous Electron Gas. *Phys. Rev.* **1964**, *136* (3B), B864–B871.
- (44) Goodenough, J. B.; Hong, H. Y.-P.; Kafalas, J. A. Fast  $\text{Na}^+$ -Ion Transport in Skeleton Structures. *Mater. Res. Bull.* **1976**, *11* (2), 203–220.
- (45) Avdeev, M. Crystal Chemistry of NaSICONs: Ideal Framework, Distortion, and Connection to Properties. *Chem. Mater.* **2021**, *33* (19), 7620–7632.
- (46) Chotard, J.-N.; Rousse, G.; David, R.; Mentré, O.; Courty, M.; Masquelier, C. Discovery of a Sodium-Ordered Form of  $\text{Na}_3\text{V}_2(\text{PO}_4)_3$  below Ambient Temperature. *Chem. Mater.* **2015**, *27* (17), 5982–5987.
- (47) Perdew, J. P.; Burke, K.; Ernzerhof, M. Generalized Gradient Approximation Made Simple. *Phys. Rev. Lett.* **1996**, *77* (18), 3865–3868.
- (48) Cococcioni, M.; de Gironcoli, S. Linear Response Approach to the Calculation of the Effective Interaction Parameters in the LDA + U Method. *Phys. Rev. B* **2005**, *71* (3), 035105.
- (49) Heyd, J.; Scuseria, G. E.; Ernzerhof, M. Erratum: “Hybrid Functionals Based on a Screened Coulomb Potential” [*J. Chem. Phys.* **118**, 8207 (2003)]. *J. Chem. Phys.* **2006**, *124* (21), 219906.
- (50) Wang, L.; Maxisch, T.; Ceder, G. Oxidation Energies of Transition Metal Oxides within the GGA + U Framework. *Phys. Rev. B* **2006**, *73* (19), 195107.
- (51) Zhou, F.; Cococcioni, M.; Marianetti, C. A.; Morgan, D.; Ceder, G. First-Principles Prediction of Redox Potentials in Transition-Metal Compounds with LDA + U. *Phys. Rev. B* **2004**, *70* (23), 235121.
- (52) Gopalakrishnan, J.; Rangan, K. K. Vanadium Phosphate ( $\text{V}_2(\text{PO}_4)_3$ ): A Novel NASICO N-Type Vanadium Phosphate Synthesized by Oxidative Deintercalation of Sodium from Sodium Vanadium Phosphate ( $\text{Na}_3\text{V}_2(\text{PO}_4)_3$ ). *Chem. Mater.* **1992**, *4* (4), 745–747.
- (53) Ishado, Y.; Inoishi, A.; Okada, S. Exploring Factors Limiting Three- $\text{Na}^+$  Extraction from  $\text{Na}_3\text{V}_2(\text{PO}_4)_3$ . *Electrochemistry* **2020**, *88* (5), 457–462.
- (54) Shannon, R. D. Revised Effective Ionic Radii and Systematic Studies of Interatomic Distances in Halides and Chalcogenides. *Acta Crystallogr., Sect. A* **1976**, *32* (5), 751–767.
- (55) Andersson, G.; Paju, J.; Lang, W.; Berndt, W. Studies on Vanadium Oxides. *Acta Chem. Scand.* **1954**, *8* (9), 1599–1606.
- (56) Pech-Canul, M. I.; Ravindra, N. M. *Semiconductors: Synthesis, Properties and Applications*; Springer: 2019.
- (57) Gopalakrishnan, J.; Rangan, K. K. Vanadium Phosphate ( $\text{V}_2(\text{PO}_4)_3$ ): A Novel NASICO N-Type Vanadium Phosphate Synthesized by Oxidative Deintercalation of Sodium from Sodium Vanadium Phosphate ( $\text{Na}_3\text{V}_2(\text{PO}_4)_3$ ). *Chem. Mater.* **1992**, *4* (4), 745–747.
- (58) Aragón, M. J.; Lavela, P.; Alcántara, R.; Tirado, J. L. Effect of Aluminum Doping on Carbon Loaded  $\text{Na}_3\text{V}_2(\text{PO}_4)_3$  as Cathode Material for Sodium-Ion Batteries. *Electrochim. Acta* **2015**, *180*, 824–830.
- (59) Zhao, Y.; Gao, X.; Gao, H.; Jin, H.; Goodenough, J. B. Three Electron Reversible Redox Reaction in Sodium Vanadium Chromium Phosphate as a High-Energy-Density Cathode for Sodium-Ion Batteries. *Adv. Funct. Mater.* **2020**, *30* (10), 1908680.
- (60) Liu, R.; Xu, G.; Li, Q.; Zheng, S.; Zheng, G.; Gong, Z.; Li, Y.; Kruskop, E.; Fu, R.; Chen, Z.; Amine, K.; Yang, Y. Exploring Highly Reversible 1.5-Electron Reactions ( $\text{V}^{3+}/\text{V}^{4+}/\text{V}^{5+}$ ) in  $\text{Na}_3\text{VCr}$

(PO<sub>4</sub>)<sub>3</sub> Cathode for Sodium-Ion Batteries. *ACS Appl. Mater. Interfaces* **2017**, 9 (50), 43632–43639.

(61) Chen, F.; Kovrugin, V. M.; David, R.; Mentré, O.; Fauth, F.; Chotard, J.; Masquelier, C. A NASICON-Type Positive Electrode for Na Batteries with High Energy Density: Na<sub>4</sub>MnV(PO<sub>4</sub>)<sub>3</sub>. *Small Methods* **2019**, 3 (4), 1800218.

(62) Ponrouch, A.; Marchante, E.; Courty, M.; Tarascon, J.-M.; Palacín, M. R. In Search of an Optimized Electrolyte for Na-Ion Batteries. *Energy Environ. Sci.* **2012**, 5 (9), 8572.

(63) Jain, A.; Ong, S. P.; Hautier, G.; Chen, W.; Richards, W. D.; Dacek, S.; Cholia, S.; Gunter, D.; Skinner, D.; Ceder, G.; Persson, K. A. Commentary: The Materials Project: A Materials Genome Approach to Accelerating Materials Innovation. *APL Mater.* **2013**, 1 (1), 011002.

(64) Bergerhoff, G.; Hundt, R.; Sievers, R.; Brown, I. D. The Inorganic Crystal Structure Data Base. *J. Chem. Inf. Comput. Sci.* **1983**, 23 (2), 66–69.

(65) Sun, W.; Dacek, S. T.; Ong, S. P.; Hautier, G.; Jain, A.; Richards, W. D.; Gamst, A. C.; Persson, K. A.; Ceder, G. The Thermodynamic Scale of Inorganic Crystalline Metastability. *Sci. Adv.* **2016**, 2 (11), No. e1600225.

(66) Bartel, C. J.; Millican, S. L.; Deml, A. M.; Rumpitz, J. R.; Tumas, W.; Weimer, A. W.; Lany, S.; Stevanović, V.; Musgrave, C. B.; Holder, A. M. Physical Descriptor for the Gibbs Energy of Inorganic Crystalline Solids and Temperature-Dependent Materials Chemistry. *Nat. Commun.* **2018**, 9 (1), 4168.

(67) Lu, W.; Wang, J.; Sai Gautam, G.; Canepa, P. Searching Ternary Oxides and Chalcogenides as Positive Electrodes for Calcium Batteries. *Chem. Mater.* **2021**, 33, 5809.

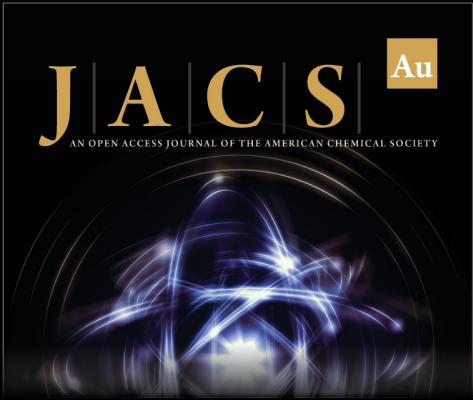
(68) Ong, S. P.; Richards, W. D.; Jain, A.; Hautier, G.; Kocher, M.; Cholia, S.; Gunter, D.; Chevrier, V. L.; Persson, K. A.; Ceder, G. Python Materials Genomics (Pymatgen): A Robust, Open-Source Python Library for Materials Analysis. *Comput. Mater. Sci.* **2013**, 68, 314–319.

(69) Ewald, P. P. Die Berechnung optischer und elektrostatischer Gitterpotentiale. *Ann. Phys.* **1921**, 369 (3), 253–287.


(70) Dudarev, S. L.; Botton, G. A.; Savrasov, S. Y.; Humphreys, C. J.; Sutton, A. P. Electron-Energy-Loss Spectra and the Structural Stability of Nickel Oxide: An LSDA+U Study. *Phys. Rev. B* **1998**, 57 (3), 1505–1509.


(71) Krukau, A. V.; Vydrov, O. A.; Izmaylov, A. F.; Scuseria, G. E. Influence of the Exchange Screening Parameter on the Performance of Screened Hybrid Functionals. *J. Chem. Phys.* **2006**, 125 (22), 224106.


(72) Ong, S. P.; Wang, L.; Kang, B.; Ceder, G. Li–Fe–P–O<sub>2</sub> Phase Diagram from First Principles Calculations. *Chem. Mater.* **2008**, 20 (5), 1798–1807.



**JACS Au**  
AN OPEN ACCESS JOURNAL OF THE AMERICAN CHEMICAL SOCIETY

 Editor-in-Chief  
**Prof. Christopher W. Jones**  
Georgia Institute of Technology, USA

**Open for Submissions** 

pubs.acs.org/jacsau  **ACS Publications**  
Most Trusted. Most Cited. Most Read.